Impact of CT-based attenuation correction on the registration between dual-gated cardiac PET and high-resolution CT

A. Turco[1], O. Gheysens[1,2], J. Nuyts[1], J.Duchenne[3], J.U. Voigt[3,4], P. Claus[3], K. Vunckx[1]

***Abstract*—A high-resolution CT (HRCT) used as anatomical prior information during PET reconstruction can enhance the quality of a corresponding low-resolution PET image, provided that it is accurately registered to the PET dataset of interest.**
In this work, the impact of different PET/CT attenuation correction (AC) protocols on the registration between a dual-gated cardiac ^{18}F-FDG PET image and an HRCT image is investigated. The aim is to explore the impact of AC on PET-to-HRCT registration, and to identify the AC strategy that yields the best alignment between the left-ventricles in the PET and the HRCT images for subsequent partial volume correction.

Simulations were performed using XCAT phantoms. Shallow breathing and a regular beating pattern were simulated and both noise-free and noisy data were evaluated.

Respiratory motion during the acquisition of the CT used for attenuation correction strongly affected the dual-gated PET reconstructions, resulting in artefacts and quantification errors in the PET image and poor PET-to-HRCT registration accuracy. The blurring introduced by the beating heart, on the other hand, proved to have a negligible effect on PET-CT registration. Dual-gated PET images reconstructed without attenuation correction could be well registered to the HRCT if a good initial alignment between the starting images was provided.
A commercially available strategy to deal with an AC CT that is acquired in the wrong respiratory phase was also evaluated, and yielded not only enhanced quantitative accuracy but also accurate PET-to-HRCT registration.
The effect of a high level of noise, as present in a dual-gated cardiac PET study, was also investigated. Registrations proved to be sensitive to noise, but noise is not a major limiting factor for PET-to-HRCT registration.

A selection of the investigated attenuation correction procedures was also evaluated using cardiac PET/CT data measured in sheep. The PET-to-HRCT registration performance confirmed the XCAT-based predictions.

[1] KU Leuven - University of Leuven, Department of Imaging and Pathology, Nuclear Medicine and Molecular imaging, Medical Imaging Research Center (MIRC), B-3000 Leuven, Belgium. [2] University Hospitals Leuven, Department of Nuclear Medicine, B-3000 Leuven, Belgium. [3] KU Leuven - University of Leuven, Department of Cardiovascular Sciences, Cardiology, Medical Imaging Research Center (MIRC), B-3000 Leuven, Belgium. [4] University Hospitals Leuven, Department of Cardiovascular Diseases, B-3000 Leuven, Belgium.

This work is supported by KU Leuven grant OT/12/084 and the Research Foundation - Flanders (FWO)

LIST OF ABBREVIATIONS

PET	Positron emission tomography
HRCT	High-resolution CT (high spatial and temporal resolution, contrast)
AC	Attenuation correction
AC CT	CT acquired and reconstructed for AC
C1-exp	ideal AC CT (end-diastole, end-expiration)
C2-exp	as C1-exp, but mismatch in the cardiac phase
C1-insp	end-inspiration AC CT (end-diastole)
AVGC-exp	AC CT averaged over the cardiac cycle (end-**ex**piration)
AVGC-insp	AC CT averaged over the cardiac cycle (end-**in**spiration)
C1-AVGR	AC CT averaged over the breathing cycle (end-diastole)
AVGC-AVGR	AC CT averaged over both breathing and beating cycle
sh(AVGC-insp)	AC CT averaged over the breathing cycle (end-inspiration), shifted
NOATTEN	no attenuation correction

I. INTRODUCTION

The measurement of ^{18}F-fluorodeoxyglucose (FDG) uptake by positron emission tomography (PET) is a validated and robust tool to investigate regional metabolism and myocardial viability [1] and can provide insights into regional myocardial workload. Limitations of the current PET imaging instrumentation can, however, compromise its diagnostic accuracy. The low spatial resolution (5-6 mm) of PET does not allow to accurately quantify the tracer uptake in very thin or small structures due to partial volume effects (PVE) [**?**], thus hampering correct estimation of glucose uptake. In addition to PVE, extracting valuable and correct information from *cardiac* images is not straightforward since the heart beats and moves in the thorax because of respiration.

The contribution of motion to cardiac images can be mitigated with different techniques [2] [3] [4]. One of the most common and straightforward methods, although not optimal for image quality, is to sort the PET dataset into a set of frames corresponding to the different phases of the periodic motion (gating), and then independently reconstruct and use each of them.

The issue related to PVE has also been frequently addressed. Among all available techniques, the application of anatomical information obtained with an HRCT or magnetic resonance imaging during the PET reconstruction with resolution modelling has been proven promising [5]. Recently, particular attention was given to brain image enhancement using the aforementioned method [6]. Even though efforts have been recently made to ensure robustness against small misalignments [7], the application of such a partial volume correction (PVC) technique to a measured PET dataset relies on a

good alignment between the anatomical image and the low-resolution PET. Hence, any source of misregistration needs to be avoided. In this scenario, PET attenuation correction might play a role in compromising the registration results.

Almost every contemporary PET scanner nowadays incorporates a CT module,that can be used to acquire a CT from which a PET attenuation map can be derived. From such map, a sinogram with PET attenuation correction factors (ACF) is obtained by forward projection and exponentiation. However, the CT for AC is often acquired at low dose and low resolution, and it is sometimes averaged over one or more breathing or beating cycles [8]. Therefore, artefacts can be introduced in the attenuation-corrected PET images, which in turn might negatively influence subsequent PET-to-HRCT registration.

To our knowledge, nothing has been reported about the influence of using a mismatched or motion-blurred map for AC on the quality of PET to high-resolution CT registration in cardiac imaging. The aim of this work is to assess the influence of attenuation correction on the quality of image registration between dual-gated cardiac PET images and high-resolution CT images, when either or both respiratory and cardiac motion are present during the AC CT acquisition. The effect of different attenuation correction strategies is investigated by means of simulations, using a realistic digital anthropomorphic phantom (XCAT [9]) and cardiac PET/CT datasets measured in sheep.

The rest of this paper is organized as follows. In Section II, the details of the phantoms used for the simulations are given, together with a description of the simulations, reconstructions, registration and evaluation methods, and real datasets. In Section III, an overview of the results obtained with noise-free and noisy datasets is presented. The results are discussed in Section IV and the conclusions are summarized in Section V.

II. Methods

XCAT-based simulations were designed to mimic a dual-gated PET study acquired on a Siemens Biograph 16 PET/CT scanner. Sinograms containing attenuation correction factors (ACF) were derived from CTs acquired on the same device using different CT protocols. Each simulated AC CT differs from the others in the way it handles the respiratory and beating motion during the scan. After gating and after performing AC, the PET frame of interest is registered to a high-resolution CT virtually acquired on a dedicated scanner, which can image the heart in a single cardiac and respiratory phase, with contract enhancement of the blood pools. The reason for this registration is to enable a subsequent anatomy-enhanced PET reconstruction for PVC. The accuracy of the registration will determine which AC CT protocols can be used if PVC is aimed for. Fig. 1 summarizes the workflow of the simulations.

A. Phantom generation

A number of XCAT thorax phantoms were generated in order to realistically simulate the HRCT, the PET and the various AC CT datasets. All attenuation and activity maps were created using a voxel size of 0.8 mm.

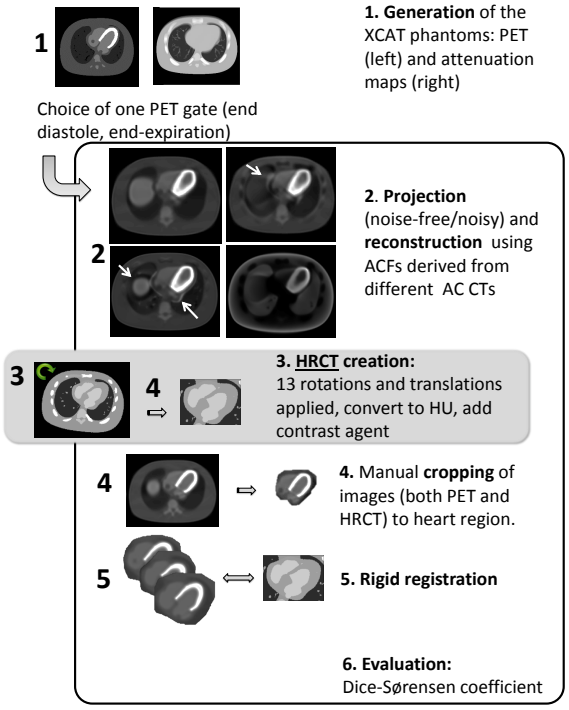

Fig. 1. Phantom generation, registration and analysis flowchart.

All phantoms represented an average male, arms up [10]. Realistic and homogeneous activity values were assigned to the different tissues of the simulated activity phantom, based on average activity values observed in available measured datasets (see Table I).

Respiratory and cardiac motion were modelled when needed. In order to be adherent to an average patient study protocol, attention was focused on the shallow breathing scenario, using the default values provided by the XCAT software [9] to describe antero-posterior (AP) expansion and diaphragm translation. A heart-rate of 60 beats per minute was also modelled. An overview of the main common parameters used to generate all the phantoms can be found in Table I.

TABLE I. Key parameters for phantom generation.

Antero-posterior (AP) expansion [cm]	1.2
Diaphragm motion [cm]	2.0
Resp. cycle duration [s]	5
Card. cycle duration [s]	1
No. resp gates/cycle	5
No. card gates/cycle	10
Phantom size [pixel]	600x600x203
Phantom pixel size [mm]	0.8
Left ventricle activity [kBq/cc]	26
Lung activity [kBq/cc]	0.9
Blood pool activity [kBq/cc]	5.5
Liver activity [kBq/cc]	6.3

This paper focuses on the registration between a dual-gated

PET image and a HRCT image in a fixed cardiac and respiratory phase. Hence, the most stable phases of the breathing and of the beating cycles were chosen for simulating these datasets. Particularly, it is known that the diastolic phase normally has a longer duration and a higher stability, compared to other phases within a cardiac cycle. Furthermore, patients with a regular shallow breathing pattern are known to spend a large amount of time in the end-expiration phase of the breathing cycle. Therefore, aiming at a doubly-gated acquisition, the choice of end-expiration phase could allow to use more data than any other phase of the breathing cycle and minimize the chances of contamination of the gate by motion (e.g. if an optimal gating strategy was used, as in [11]). For this reason, the HRCT and the dual-gated PET image of interest are simulated to be acquired in the end-diastolic cardiac phase and in the end-expiration breathing phase.

More details about the different datasets are given in the following of this section.

HRCT dataset: In order to generate the HRCT frame of reference, a dataset with blood-pool contrast and high spatial and temporal resolution was generated. The cardiac cycle of the XCAT phantom was divided into 10 equally spaced time frames (gates), for a total cycle duration of 1s. The gate corresponding to end-diastole was chosen, while the other frames produced with the XCAT phantom were discarded. The respiration phase of the simulated HRCT phantom was kept fixed to end-expiration. This image, generated with the XCAT software, was converted to Hounsfield units and small rotations and translations were applied to it, to simulate patient positioning differences between the PET/CT scan and HRCT scan. Thirteen different initial roto-translations were simulated, where the sets of three rotation and three translation values were obtained by randomly sampling a uniform distribution of rotation and translation values in the range of [0, 0.3] rad and [0, 4] cm respectively. The resulting HRCT images served as the target high-resolution CT, to which the PET frame of interest should be registered.

PET dataset: The phantom from which the HRCT dataset was extracted was also used to obtain the corresponding PET dataset. The selected PET frame, therefore, was the one that captured the heart in end-expiration and end-diastole.

AC CT datasets: Additional phantoms were generated to obtain various attenuation maps (see also Fig. 2), which differ in the way the AC CT is acquired in the presence of the cardiac and respiratory motion.

- **C1-exp** : the attenuation map perfectly matches the PET respiratory and cardiac phase, thus leading to **ideal**, artefact-free PET reconstructions.
  In practice, this can be obtained with a very fast CT scan or with a medium speed CT scan coupled with ECG-gating during breath-hold. However, a cardiac-gated CT results in a higher dose for the patient. In addition, a breath-hold in end-expiration, for an amount of time sufficient to acquire such AC CT, can be difficult for many patients. Therefore, C1-exp is not the most desirable protocol in clinical practice. For this reason, other AC CT protocols have to be considered.

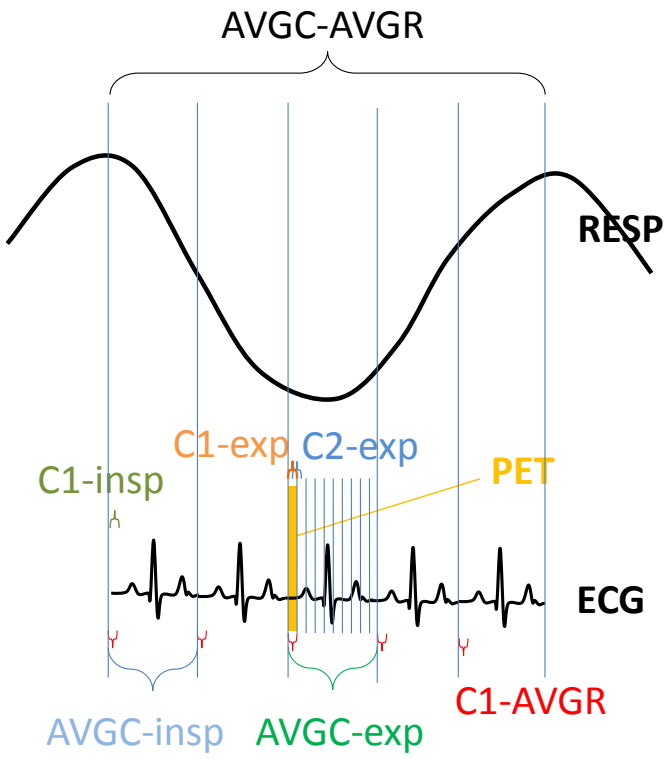

Fig. 2. ACCTs generated with the XCAT software and their position with respect to cardiac and respiratory motion.

- **C2-exp** : similar to *C1-exp*, but the attenuation map is **slightly mismatched** with respect to the **cardiac phase** of the corresponding PET image.
- **C1-insp** : similar to *C1-exp* the beating phase of the CT for attenuation correction corresponds to the one of the PET and the HRCT, but it is simulated to be in a completely **different respiratory phase** (i.e., end-inspiration, because breath-hold in this phase is typically easier for patients).
- **AVGC-exp** : the AC CT corresponds to the **average over** a complete **heart cycle**. This is equivalent to a breath-hold CT acquired at end-expiration.
- **AVGC-insp** : similar to *AVGC-exp*, but the **respiratory phase is different** (i.e., end-inspiration instead of end-expiration). Since this AC CT is an average over one full beating cycle, it represents the result of a CT acquired at medium scanning speed with breath-hold.
- **C1-AVGR**: the AC CT perfectly corresponds to the cardiac gate of the PET being reconstructed, but it is **affected by** motion blur due to **respiration**. This AC CT could be the result of an ECG-gated CT acquired during free breathing with a low pitch.
- **AVGC-AVGR**: an AC CT obtained by **averaging** all AC CTs **over** one **breathing and** several **beating** cycles was obtained with the XCAT software. This would correspond to a scenario where the patient is breathing regularly during a CT acquisition with a very low pitch.
- **sh(AVGC-insp)** : the same AC CT as *AVGC-insp* is

used. However, it is **aligned to the PET dataset before using it for AC** of the PET dataset. In order to align the myocardium of the AVGC-insp image to the myocardium of the PET image, binary masks corresponding to the myocardium were automatically generated, both in the PET and in the AC CT. For simplicity, the delineation of the myocardium in the AC CT was performed by thresholding the corresponding gate of the *activity* map to the myocardial tissue. The mask image corresponding to the AC CT was subsequently rigidly registered (only translations allowed) to the PET mask image using normalized cross-correlation. The registration parameters were then applied to the AVGC-insp and the resulting, shifted attenuation map ('sh(AVGC-insp)') was used for attenuation correction. This procedure is only possible in a simulation study. In practice, the creation of such mask images could be cumbersome, especially for what the AC CT is concerned. The most practical solution in this case, currently implemented on several PET/CT systems from various manufacturers, is to proceed with a rough manual alignment of the myocardium of the AC CT to the myocardium of the PET [12] [13].

- **NOATTEN** : as a final alternative, the PET gate was also reconstructed **without any attenuation correction**.

B. Projection and reconstruction of the activity phantom

The image generated with the XCAT software and corresponding to the PET gate of interest was projected using in-house developed software that simulates an acquisition with the PET component of a Siemens Biograph 16 PET/CT (Hirez) scanner [14]. Attenuation and a shift-invariant camera resolution were modelled, but scatter and randoms were not.

A noise-free sinogram was obtained. In addition, ten noisy sinograms were generated by adding Poisson noise to the noise-free sinogram, corresponding to a 36 s-acquisition. The rationale behind this value is as follows. An average PET scan can last up to 30 minutes. If motion-free images need to be obtained, the easiest way is to perform a double gating pass on the original listmode data set. This way, the initial dataset is first divided into, e.g., 5 respiratory gates, and after that every respiratory gate is further divided into, e.g., 10 cardiac gates. Thus, a 30-min PET scan must be equally divided into 50 gates, resulting in an actual contribution of 36 s to each gate.

In order to verify whether shorter scan times influence the results obtained, we additionally generated noisy PET reconstructions with lower count levels. Particularly, Poisson noise was added to the noise-free sinogram to simulate 6 s-, 12 s-, 24 s- and 30 s-acquisitions, which correspond to a total scan time of 5, 10, 20 and 25 minutes respectively. The activity sinogram was then reconstructed using a 3D OSEM algorithm with resolution recovery (4 iterations and 12 subsets per iteration). Projection and backprojection were done using ray tracing, modelling the system resolution as a shift-invariant Gaussian convolution (FWHM = 4.3 mm and 4.5 mm in the transaxial and axial direction, respectively). The voxel size of the reconstructed PET images was set to 2 mm x 2 mm x 2 mm. The different AC CTs, described in Section II-A, were converted to PET attenuation maps with voxel size of 0.8 mm x 0.8 mm x 0.8 mm. Sinograms containing the ACFs were computed from the forward projection of these maps with a ray tracing projection method. Each of those sinograms was used during each iteration of the reconstruction to correct for the effect of attenuation. The same reconstruction procedure was applied to the noisy sinograms.

C. Image pre-processing

The reconstructed noisy and noise-free PET datasets were roughly cropped to the heart region, by manually delineating the region of interest (ROI) in the central transaxial slice of each volume and automatically propagating the same ROI to all other image planes. The cropping procedure was found to be beneficial for registration and drastically reduced the total computation time [15]. The shape of the cropped ROI was arbitrary as long as it contained the whole heart, both axially and transaxially. All PET reconstructions received the same cropping, in order not to influence registration results with an additional, possible source of variation. The thirteen roto-translated HRCT images were manually cropped too, with a different cropping for each HRCT, and not identically as the cropped PET images.

D. Quantification of image artefacts

Various degrees of artefacts are to be expected in the reconstructed PET images, depending on the attenuation map used for reconstruction. The reconstruction with C1-exp is here regarded as the gold standard, because it perfectly matches both the respiratory and the cardiac phase of the corresponding PET, yet being more realistic than the initial phantom as projected and reconstructed with software that simulates the behaviour of the scanner.

As a measure of the severity of the artefacts in the heart region, we computed difference images between the PET images corrected with the various attenuation maps and the PET image corrected with C1-exp. Moreover, the sum of squared differences between such images was also calculated, after cropping the datasets as explained in II-C.

E. Quantification of activity

In those fields where accurate quantification of the activity is required, attenuation correction might play a role in under- or over-estimating activity values in the region of interest. In this work, the reconstructed activity within the left ventricle (LV) is of interest. For this reason, the quantification accuracy of the total reconstructed activity within the LV in the PET images corrected with the various ACF sinograms was also briefly investigated.

First, the total reconstructed activity in the LV was calculated. Based on the XCAT phantom, a binary mask images was created, where the LV was set to 1 and all other image pixels were set to 0. All the reconstructed, noisy PET datasets, corrected with the various AC CTs, were then multiplied by such mask, and the total activity was calculated. The mask

used is one for all PET reconstructions. We opted for this strategy in order to clearly evaluate the artefacts within the original LV region. The other approach, that is to optimize the mask for each PET corrected with a different AC CT, introduces increased chances of hiding the artefacts produced by the various AC CTs.

The mean total activity over the ten noise realizations was calculated. A paired t-test was performed between the values obtained in the (ideal) case of PET images corrected with C1-exp and with each of the other ACF sinograms. C1-exp was chosen as ground truth, instead of the phantom, in order to rule out any possible effect of the reconstruction process on the results.

In addition, the quantification of the LV was evaluated for an artificially-created AC CT. In case the HRCT was registered directly to the NOATTEN PET, because no suitable AC CT was available for accurate image registration (see Section III-C), quantification could be performed on a subsequent PET reconstruction using the aligned HRCT as AC CT. However, often the HRCT available does not cover the full field-of-view (FOV) being imaged. Therefore, it would be necessary to paste such HRCT into the corresponding region of a full-FOV AC CT (acquired at low-resolution, low-dose) in order to have all the necessary information for performing AC on the full-FOV PET image. Such a scenario was simulated with the help of the XCAT phantom by 'pasting' a cropped high-resolution CT, deprived of blood-pool contrast, into a full-FOV AVGC-AVGR. The simulated PET gate of interest was then reconstructed using such a 'pasted-HRCT', and the effect of the discontinuities on the LV quantification was studied.

Additional analyses were also performed on the most interesting AC strategies: C1-exp, AVGC-AVGR, AVGC-exp, sh(AVGC-insp) and pasted-HRCT. C1-exp was chosen as the reference or gold standard. The AVGC-AVGR and AVGC-exp were further studied because they would be the easiest to perform in the clinical practice. The sh(AVGC-insp) has a promising potential of restoring the total LV activity to values closer to the reference. Finally, the pasted-HRCT would be the only reason to justify the registration of NOATTEN PET datasets to the HRCT.

For this purpose, a 17-segments polar map [16] was generated for each of the noisy PET reconstructions corrected with ACFs derived from the aforementioned AC CTs. For visual assessment, the average activity value over the 10 noise realizations was computed, for each segment of each polar map. For a more quantitative assessment, a value describing the uniformity of each of the polar maps was defined as follows:

$$R_s = \frac{\bar{x}_s}{\bar{x}}, s = 1...17$$
$$U = stddev(R)$$

with $R = [R_1, .., R_{17}]$. In other words, the ratios between the mean activity value in each of the segments ($\bar{x}_s$) and the mean overall activity value ($\bar{x}$) was computed, for each segment of each attenuation strategy. The closer these ratios to 1, the more uniform the polar map is. The standard deviation U of these ratios over the 17 segments was then computed. The closer U to 0, the less the ratios are spread around the value of 1 (ideal, perfectly uniform polar map), thus giving an indication on the LV uniformity.

Wall ratio calculations were also performed to quantify more regional changes in uniformity. To this end, the average polar maps were divided in 5 areas, corresponding to the anterior wall (segments 1, 7, 13), posterior wall (segments 4, 10, 15), lateral wall (segments 5, 6, 11, 12, 16), septum (segments 2, 3, 8, 9, 14) and apex (segment 17). The mean activity in each of these regions was calculated, and the antero-posterior (AP) and lateral-septal (LS) wall ratios were then computed.

F. Registration approach

Rigid registration of the PET frame to the HRCTs was performed using the cropped images. Normalized mutual information (NMI) was chosen as the matching criterion, since it has been proved particularly effective for inter-modality image registration of cropped datasets [17]. Registration was performed in three steps, in a multiresolution fashion. One hundred bins were used to histogram the intensity ranges of the images being registered. This value was chosen to ensure a clear distinction of the intensities of the LV and the blood pools both in the PET and in the HRCT images.

Poor registration results were obtained at times. In order to exclude from the causes of this failure the initialization of the PET dataset, whose initial orientation was relatively different from that of the HRCT image, a preliminary image alignment was attempted. To this end, we performed the same PET-to-HRCT registrations, but starting from parameters that yielded a very good initial positioning of the PET dataset if compared to the orientation of the HRCT. A drift from this initial and ideal positioning during the registration process would confirm the role of the artefacts in hampering the registration outcome.

For the NOATTEN datasets, which were the only ones that proved to benefit from such initialization, a manual preliminary alignment was also attempted. This procedure, albeit less accurate, provided a more viable and realistic alternative to roughly initialize the datasets of interest.

G. Evaluation of registration results

Evaluation of PET-to-HRCT registration was done in PET space, as this will be the space where PVC is applied. The registered images were evaluated visually and quantitatively. DICE-Sørensen coefficients (DSC) were calculated to quantify the overlap between the left ventricular region in the PET image and the LV region in the registered high-resolution CT. For this purpose, the same mask images as for quantification were used (see Section II-E) and the overlap between them was measured by means of the DSC.

Since the evaluation needed to be performed in PET space, but only the parameters corresponding to PET-to-CT registration were available, the inverse registration transformations were applied to the CT mask before calculating the DSCs.

H. Real datasets

Finally, we verified whether the findings from the simulation studies found correspondence with results obtained on sheep.

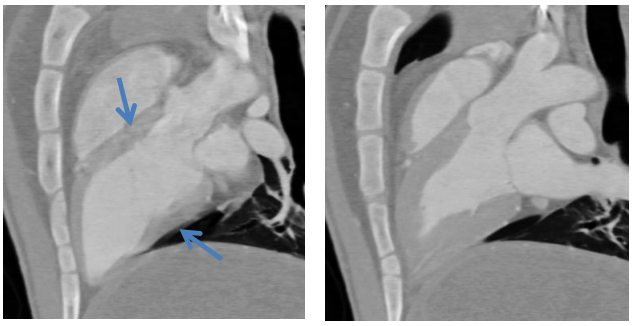

Fig. 3. Comparison between a HRCT affected (left) and not affected (right) by motion blur. The slice is representative for the whole volume.

To this purpose, two sheep experiments approved by the local ethical committee were carried out. Detailed information on the two animals, together with an overview of the settings used during the scans, are in table II.

TABLE II. KEY INFORMATION ON THE ANIMAL EXPERIMENTS.

General information	
Weight, sheep 1 [kg]	42.0
Weight, sheep 2 [kg]	55.0
Age, sheep 1 [days]	345
Age, sheep 2 [days]	376
HRCT generation parameters	
Scanner	Siemens SOMATOM Definition AS
kVp	120
mAs	257
pitch	0.34
PET scan information	
^{18}F-FDG administered dose, sheep 1 [MBq]	374,30
^{18}F-FDG administered dose, sheep 2 [MBq]	237,12
scan time [min post-injection]	30
scan duration [min]	30

Each sheep underwent the following scans (all at constant heart rate of 110 beats per minute):

1) a high-resolution CT with contrast enhancement acquired on a Siemens SOMATOM Definition scanner, using a pre-defined ECG-gated spiral protocol (CoronaryCTA). Ten different cardiac gates were reconstructed. The respiratory phase during which the whole dataset was acquired was known and represented end-expiration. One volume corresponding to one cardiac phase was selected, thus obtaining a real HRCT where the heart is in a fixed and known respiratory and cardiac position.
   The cardiac phase was chosen based on a visual analysis of the entire HRCT, i.e., the cardiac gate that showed the least amount of motion and contrast-related artefacts in the LV region was chosen. In fact, it was observed that the use of a HRCT in which the uniformity of the LV was compromised and the distinction between the LV walls and the LV chamber was less neat (e.g. left pane of Fig. 3) resulted in poor registration outcomes. In the animals, the respiratory phase during which the HRCT was acquired was obtained by means of a mechanical ventilator. In patient studies, a fixed respiratory phase could be obtained by means of an active breathing control system (as in [18]).
2) a 30-minute ^{18}FDG-PET scan, acquired on the Siemens Biograph 16 (Hirez) scanner. Triggers corresponding to both the cardiac (ECG) and the respiratory signal (from the Respiratory Gating System AZ-733V) were inserted into the listmode during acquisition, and subsequently used to double-gate the dataset using in-house software. A phase-based gating approach was used for the respiratory motion, as the respiration of the sheep was artificially controlled by a ventilator, hence very regular in its pattern. The chopped listmode data corresponding to the same cardiac and respiratory phase as the best HRCT gate was selected, by taking the end-expiration chunk and selecting the same cardiac phase according to the ECG triggering. Such short listmode was converted to a sinogram and reconstructed using the different attenuation maps listed in the remainder of this section.
3) different AC CTs, acquired on the Siemens Biograph 16 (Hirez) scanner:
   a) an average low-dose AC CT at low pitch, hence spanning over multiple cardiac and respiratory cycles. This acquisition corresponds to the AVGC-AVGR AC CT simulated with the XCAT phantom.
   b) an average low-dose AC CT at low pitch, again spanning over multiple beating cycles. However, differently from a), the respiratory phase in which this AC CT was acquired was known and fixed to end-expiration. Such acquisition mimics the AVGC-exp simulated with the XCAT.
   c) a cardiac-gated CT acquisition at low pitch, thus spanning over multiple respiratory cycles. This CT resembles the C1-AVGR.
   d) a cardiac-gated CT acquisition, when the respiration of the sheep is forced to end-expiration, reproducing the behaviour of the simulated C1-exp.

All the AC CTs were converted to 511 keV attenuation maps using the hybrid scaling method [19], forward-projected using in-house software that simulates the behaviour of the PET scanner and used as AC sinograms during the reconstruction of the selected PET gate. One PET reconstruction was performed without any attenuation correction, too. The activity sinogram was reconstructed using a 3D OSEM algorithm with resolution recovery (4 iterations and 12 subsets per iteration). The voxel size of the reconstructed PET images was set to 1.35 mm x 1.35 mm x 2 mm.

Each of the resulting reconstructions was manually cropped to the heart region (as for the simulation study, only transaxial cropping was performed). The HRCT from the dedicated, high-resolution scanner was cropped as well to delineate the heart. All PET reconstructions of the same sheep received the same cropping, but PET and HRCT were cropped differently.

Finally, the cropped PET datasets were registered to the cropped HRCT. The resulting registrations were evaluated by visual inspection.

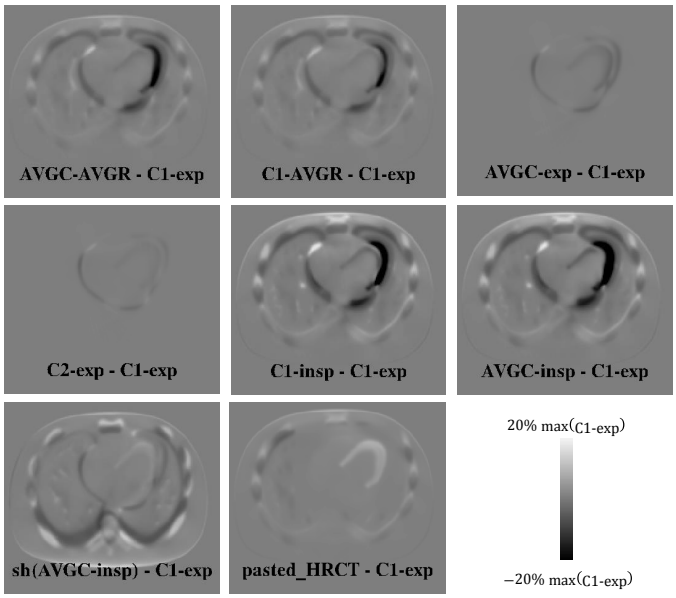

Fig. 4. PET reconstructions corrected with C1-exp subtracted from the PET datasets reconstructed with different attenuation maps. Clear artefacts are present, both around and within the myocadium.

III. Results

A. Quantification of image artefacts

Fig. 4 shows the artefacts that can be caused by using different AC CTs in the simulated noise-free datasets. Table III confirms what can be intuited from the images. A high SSD (sum of squared differences) is obtained when the artefacts are more pronounced.

TABLE III. SSD between the cardiac region of the PET reconstructions (corrected with the ACF derived from the different AC CTs) vs the ideal reconstruction (C1-exp)

	SSD
AVGC-AVGR	6.83e+11
C1-AVGR	6.19e+11
AVGC-exp	2.74e+10
C2-exp	1.22e+10
C1-insp	1.92e+12
AVGC-insp	2.07e+12
sh(AVGC-insp)	3.48e+11
pasted-HRCT	9.40e+10

B. Quantification of accuracy

The total activity was calculated within the LV wall of the different attenuation-corrected, noisy PET reconstructions. The results are summarized in Table IV. Although the artefacts produced by the use of different attenuation maps are not always visually striking, the AC CT used does have an effect on the total reconstructed activity within the LV. Moreover, a procedure to align the myocardial volumes in the AC CT to that in the PET before the PET reconstruction (sh(AVGC-insp)) seems to be beneficial when compared to the reconstruction using the un-shifted version of the same attenuation map ('AVGC-insp'). The usage of a 'pasted-HRCT' AC CT overestimated the overall activity.

TABLE IV. Mean activity values in the LV, for the PET reconstructed with different attenuation maps.

	Mean act. LV [MBq]	% act. difference from C1-exp	p-value
AVGC-AVGR	3.945 ± 0.111	-4.8%	7.6E-19
C1-AVGR	4.033 ± 0.113	-2.7%	2.6E-14
AVGC-exp	4.076 ± 0.115	-1.7%	1.4E-10
C1-exp	**4.144 ± 0.115**	-	-
C2-exp	4.136 ± 0.116	-0.3%	0.17
C1-insp	3.848 ± 0.110	-7%	5.6E-22
AVGC-insp	3.692 ± 0.109	-10.9%	2.5E-25
sh(AVGC-insp)	4.276 ± 0.120	+3.4%	1.9E-15
pasted-HRCT	4.317 ± 0.120	+4.5%	1.4e-17

Fig. 6 shows the polar map analysis. Uniformity is best preserved when C1-exp (gold standard) and AVGC-exp are used, whereas AVGC-AVGR shows the largest variations. Using a 'pasted-HRCT' also seems to preserve uniformity, and yields improvements when compared to the usage of AVGC-AVGR. The U-values calculated for each polar map, together with the wall activity ratios presented in table V, confirm such findings.

The best compromise between preservation of total activity and uniformity is obtained when using AVGC-exp as AC CT for deriving the ACF sinogram.

TABLE V. U-values and wall ratios, calculated on the average polar maps.

	AP ratio	LS ratio	U-value
AVGC-AVGR	1.067	0.942	0.054
AVGC-exp	1.055	1.003	0.033
C1-exp	**1.031**	**1.015**	**0.030**
sh(AVGC-insp)	1.067	1.007	0.0417
pasted-HRCT	0.983	1.015	0.034

C. Registration

In multimodal image registration, (N)MI has become a technique of reference. To our knowledge, however, the effect of the mis-alignment between the anatomical and emission image on PVC *for cardiac imaging* has not yet been addressed in previous literature.

Alignment tasks using MI for PET and MR images have shown an accuracy below 2 mm in brain [20]. Slightly worse accuracy values can be expected in cardiac imaging, where residual motion present in the datasets might deviate the registration algorithm from the optimal solution. On the other hand, the accuracy of the registration between ungated whole-body PET and CT is pretty low (around 5-6 mm in the thorax) [21], but we believe these accuracy values can be improved with the application of double gating on the emission datasets.

A small simulation study allowed us to establish a rough correlation between the DSC of two simulated emission images of the LV and a mono-directional shift progressively applied to one of the two. Fig. 5 illustrates the result. The DSC decreases linearly with increasing shift values. Shifts in the three different directions were tested, with comparable results.

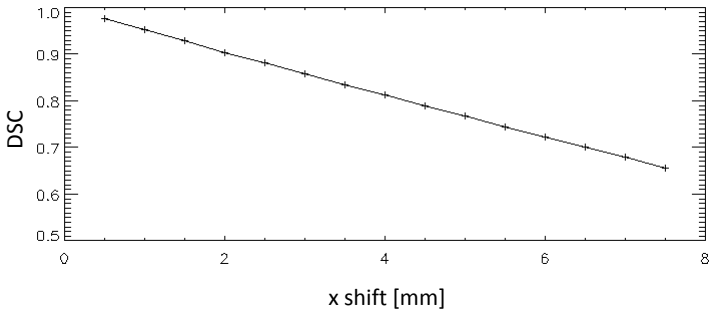

Fig. 5. DSC obtained by overlapping a reference image of the LV to its shifted versions. Increasing shift values were tested, ranging from 0.5 mm to 7.5 mm.

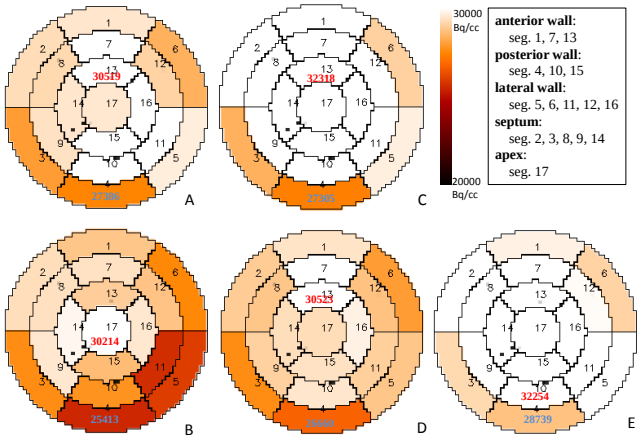

Fig. 6. Average 17-segments polar maps for the simulation study. The value assigned to each segment is the mean value of the segment, averaged over 10 noise realizations. PET corrected with (A) C1-exp, (B) AVGC-AVGR, (C) sh(AVGC-insp), (D) AVGC-exp, (E) pasted-HRCT

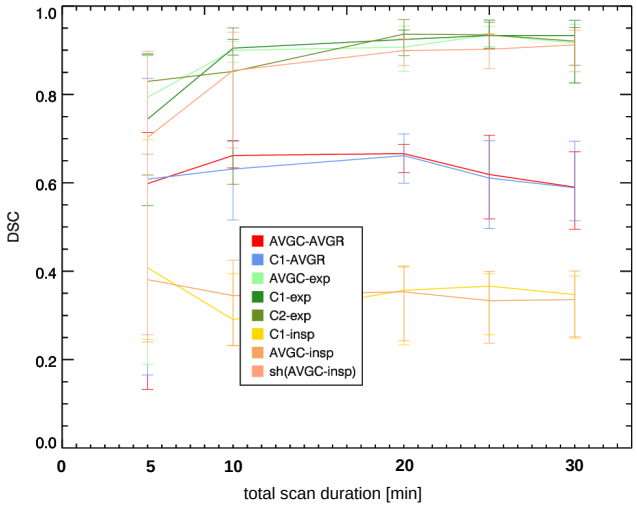

Fig. 7. Mean DSCs and min-max errors after PET-to-HRCT registration. The duration of the PET gates is progressively increased from 6s/gate (corresponding to a 5-min total scan duration, doubly-gated with 5 respiratory and 10 cardiac gates) to 36s/gate (corresponding to a 30-min total scan time).

Effect of AC: From the registration results of the noise-free as well as of the noisy datasets, we can conclude that the use of different attenuation maps does play a role in the final registration outcome. Fig. 8 shows the amount of overlap after aligning the PET images reconstructed with the different ACF sinograms to the HRCT. Both in the noisy and in the noise-free case, the blur introduced by the beating of the heart does not influence the subsequent registration to the HRCT (cfr. AVGC-exp and C1-exp). In the light of the findings illustrated in Figure 5, the DSC values obtained in these cases correspond to a mismatch of less than 2 mm between the PET and the HRCT, compatible with the best performances of the currently available registration techniques and below the PET resolution (about 4.5 mm FWHM). On the other hand, a mismatch in the respiratory phase during which the AC CT is acquired does influence the subsequent PET-to-HRCT registration (e.g. see C1-insp and C1-AVGR vs C1-exp).

Evident artefacts could already be noted in the difference images presented in Fig. 4, and from the values shown in table III. The reconstructions with the highest SSD values also produced the worst registration results, thus allowing to establish a relationship between artefacts introduced by the attenuation process and final registration outcome.

Noise contribution: When noise is added to the PET datasets, the trend is maintained. A simulation of the PET with different count levels shows that we can even decrease the total scan duration down to 20 minutes, without affecting the registration outcome. Figure 7 illustrates the findings. When scans of very short duration are simulated, i.e. 5 and 10 minutes (corresponding to 6 and 12 s-duration per gate), we can notice a general increase of the variance and a decrease of the mean of the DSC values for almost all AC strategies. The decrease in performance at higher counts for AVGC-AVGR and C1-AVGR might be explained by the fact that, at lower noise levels, the artefacts introduced by the wrong respiratory phase are also more crisp and less confounded with noise, and therefore hamper more the registration. The DSCs obtained are anyway not acceptable for PVC.

In order to get rid of the slight decrease in performance introduced by the presence of noise, a smoothed version of the PET images was generated and used for subsequent registration to the HRCT. The results, presented in Fig. 8, confirm that improved DSCs can typically be obtained if the PET is smoothed with a Gaussian kernel of 4.3 mm (equal to the detector resolution), except if the PET datasets were reconstructed without AC (i.e., NOATTEN).

Robustness to initial positioning: The robustness of the AC strategies to the initial difference in position between the PET and the HRCT was also analysed. Thirteen different rotations and translations were applied to the HRCT before registering it to the PET datasets corrected with the different ACF sinograms. Fig. 9 shows the results obtained when noise-free datasets are considered. Results proved to be fairly robust against different initializations of the HRCT dataset, except when NOATTEN datasets were used (last column in Fig. 9). In order to improve the un-satisfactory results obtained

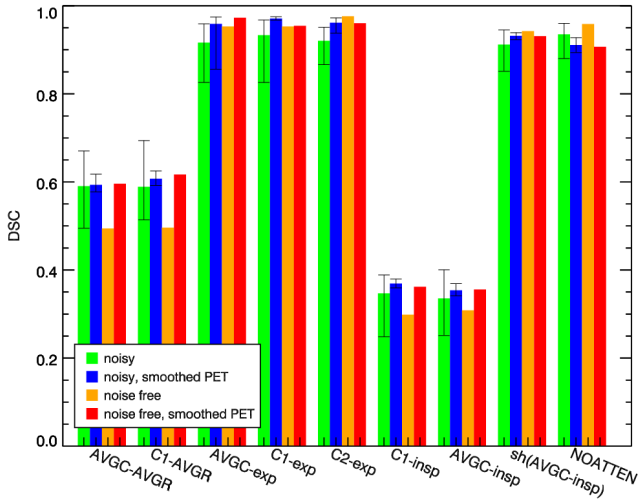

Fig. 8. Mean, minimum and maximum DSC values over **10 noise realizations**, for **different AC strategies** and a 30-min PET scan time. Cardiac motion is irrelevant, whereas the choice of the right respiratory phase is mandatory to achieve an acceptable final overlap (DSC $\geq$ 0.9). PET **smoothing helps** to improve overall image alignment.

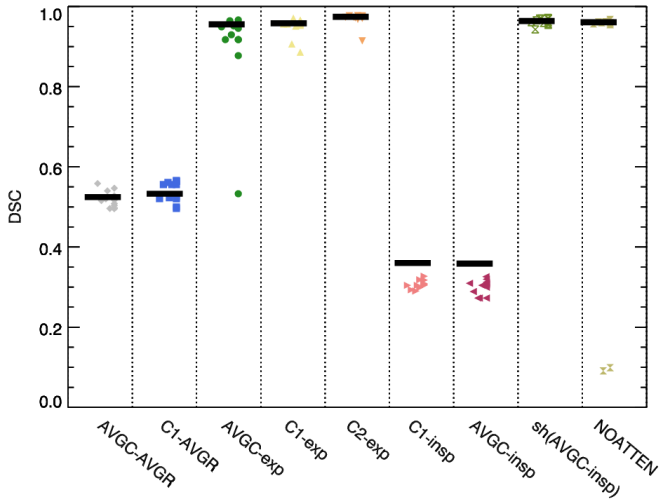

Fig. 9. Effect of **different initial positions (parms 0-12)** of the HRCT on the PET-to-HRCT registration (noise-free datasets). Each point cloud stands for a different AC strategy. Each point in a cloud represents the result of the registration of the PET to a HRCT roto-translated with a different set of parameters (0-12). The black line represents the result of the registration with an ideal initialization of the datasets.

with AVGC-AVGR, C1-AVGR, C1-insp and In-C1-AVGR, the effect of the initial rotation was undone by initializing the PET-to-HRCT registration with a good parameter set, as explained in Section II-F. The results obtained after the initial alignment did not change, compared to the case where un-initialized registrations were performed. Only NOATTEN datasets seemed to benefit from such procedure (see Fig. 9, solid black line).

NOATTEN datasets: The NOATTEN PET-to-HRCT registration can be as good as in the ideal case of C1-exp-to-HRCT, but it can also be very poor (see Fig. 9), showing that the registration outcome depends on the initial alignment between the PET and the HRCT. Possible strategies to overcome the problem were evaluated, including an initial, rough manual alignment of the two volumes of interest, an initial HRCT-to-AC CT (AVGC-AVGR) automatic rigid registration or an histogram equalization of the NOATTEN-PET. The initial manual alignment produced the best results (results not shown).

The addition of noise increased the instability of the registration results in the NOATTEN case. Again, a rough manual alignment mitigates the problem (not shown).

sh(AVGC-insp) datasets: When aligning the PET corrected with AVGC-insp to the HRCT, a low registration accuracy is achieved, both in the noise-free and in the noisy case, due to the artefacts produced by the difference in respiratory phases between the PET and the AC CT (see Fig. 8, AVGC-insp). A procedure that can be rather easily applied in the clinic is therefore to align the AC CT to the PET before applying the new, shifted AC CT for attenuation correction, as described in Section II. The AC CT alignment can be manual or automatic. In this simulation study, the automatic alternative was chosen for simplicity. Fig. 10 and Fig. 8 show the registration accuracy obtained with this shifted attenuation map (sh(AVGC-insp)). The sh(AVGC-insp) procedure yields

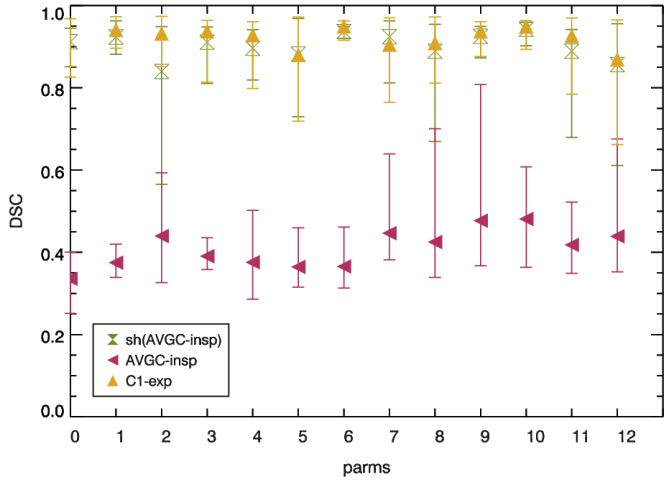

Fig. 10. Mean, minimum and maximum DSC values over 10 noise realizations, for 13 different initial HRCT rotations. Cropped images, shallow breathing, PET-to-HRCT registration. The results of the **sh(AVGC-insp)** procedure are shown **in comparison with** the non-shifted version of the same AC CT (**AVGC-insp**), and to the ideal case of a perfectly matching AC CT (**C1-exp**).

markedly improved registration to the HRCT, when compared to the usage of the un-shifted version of the same attenuation map (i.e. AVGC-insp). These improved results are very similar to those obtained with the ACF sinogram derived from the perfect AC CT (i.e. C1-exp).

D. Real datasets

The results obtained for the sheep datasets confirmed those predicted by the XCAT simulations (see Fig. 11). In the first

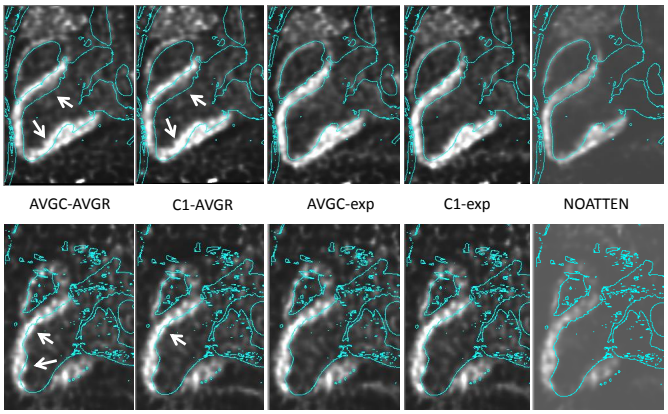

Fig. 11. Results of the registration between double-gated PET sheep datasets corrected with the ACF sinograms derived from the different AC CTs and the HRCT obtained for the same animal in the corresponding cardiac and respiratory phase. Each column represents the result of the registration of PET images corrected with different ACF sinograms. The blue contours are from the HRCT. Top row: sheep no.1, Bottom row: sheep no.2.

sheep the results are striking, whereas for the datasets acquired with the second sheep the effects of AC on PET-to-HRCT registration are less pronounced. In both cases, however, a PET image corrected with an attenuation map that matches its respiratory phase results in the best alignment with the HRCT, regardless whether the cardiac phase was matched or not. On the other hand, the use of an AVGC-AVGR AC CT yielded clear misalignment, which is in agreement with the results obtained with the XCAT simulations. The polar maps of the first sheep, together with a table reporting uniformity values and AP-LS ratios, are also included in this study and shown in Fig. 12 and table VI respectively. The ratios and the uniformity values are most similar to the ideal attenuation-corrected PET (C1-exp) when the ACCT is acquired in a fixed respiratory phase, cfr. ACGC-R1 and AVGC-AVGR.

TABLE VI. U-VALUES AND WALL RATIOS FOR THE FIRST ANIMAL DATASET.

	AP ratio	LS ratio	U-value
AVGC-AVGR	1.034	1.24	0.0649
AVGC-exp	1.036	1.27	0.0584
C1-exp	**1.043**	**1.270**	**0.0598**
C1-AVGR	1.037	1.249	0.0636

The usage of C1-AVGR hampered an accurate registration between volumes acquired with the first sheep, whereas for the second sheep the differences in terms of registration outcome, if compared to the registrations of the PET corrected with e.g. C1-exp, are less obvious. This may be partially due to the fact that the first sheep dataset was acquired in optimal conditions and on a healthy animal. The second dataset available, on the other hand, was acquired on a diseased sheep (myocardial infarction). In addition, a visual inspection of the C1-AVGR for the second sheep revealed that this scan was probably performed at a moment when the sheep was not breathing enough to produce visible blur or motion artefacts.

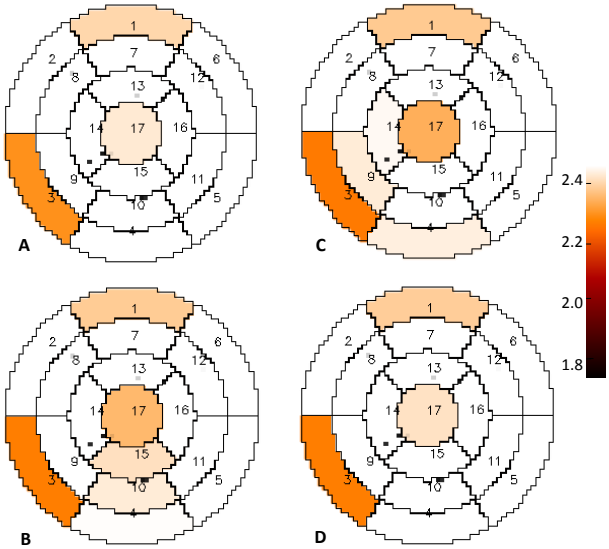

Fig. 12. Average 17-segments polar maps for the first sheep dataset (SUV values). The value assigned to each segment is the mean value of the segment. PET corrected with (A) ideal ACCT (C1-exp, reference), (B) AVGC-AVGR, (C) C1-AVGR, (D) AVGC-exp

IV. DISCUSSION

The present work addresses one of the problems introduced by the attenuation correction process, when the breathing and beating motions of the heart are taken into account. In particular, it analyses the effect of the attenuation artefacts produced on the reconstruction of an ^{18}F-FDG PET dataset, on a subsequent registration to an HRCT for partial volume correction purposes.

An accurate PVC of the emission datasets could, in turn, improve the diagnostic quality and the quantitative information of cardiac ^{18}F-FDG PET images. This could have an impact on several clinical conditions as exemplified below.

First of all, even though both delayed-enhancement MRI (DE-MRI) and ^{18}F-FDG PET have been recommended for viability assessment [22], DE-MRI is increasingly used and has nearly replaced FDG-PET. However, ^{18}F-FDG PET is still used for viability assessment in a conspicuous number of patients, particularly those that cannot undergo an MRI scan (e.g. due to pacemakers, implanted defibrillators, claustrophobia).

In addition, ^{18}F-FDG PET is not limited to assess viability in heart failure patients, but can also provide metabolic information in patients with conduction delays. Cardiac resynchronization therapy (CRT) with bi-ventricular pacemakers has become an accepted treatment in patients with conduction delays (eg. dilated cardiomyopathy), but more than one third of the patients selected for CRT with the available guidelines fail to respond to the treatment [23], [24]. Hence, better predictors for adequate therapy or new guidelines are needed to avoid unnecessary implantations. Recently, a relationship between inhomogeneous glucose uptake and delayed LV activation has been observed in patients with dilated cardiomyopathy, suggesting that ^{18}F-FDG PET might be used as a tool for better

patient selection for CRT [25]–[27]. However, the limited spatial resolution of the PET scanners currently available might not allow to distinguish a thin myocardial wall with normal metabolism from a thick wall with reduced metabolism due to possible partial volume effects. Therefore, the use of additional morphological information from other imaging modalities (eg. HRCT) to correct for PVC might give a better insight into the true activity distribution of the ^{18}F-FDG PET and, as a consequence, improve its predictive value. In order to perform this partial volume correction, a necessary step would be to accurately align the PET emission and the anatomical datasets. This work underlines the need for using an appropriate AC CT to achieve a satisfactory image alignment, which is a necessary condition for accurate PVC.

Nowadays, dedicated CT scanners with high spatial and temporal resolution entered the clinical practice. These scanners are able to image the heart in a 'frozen' cardiac and respiratory phase with a significantly reduced radiation burden for the patient [28], thus avoiding the acquisition of a dedicated, high-dose HRCT. In addition, the methodology used in the current work could be extended to other imaging modalities as source of morphological information, such as MRI, instead of HRCT. This would exclude the need of a dedicated HRCT scan, and further reduce the radiation burden for the patient.

Finally, the emission images obtained with various other tracers could benefit from the results of this study, especially if the tracer distribution and the signal-to-noise ratio in the heart region is similar to that in an ^{18}F-FDG PET image. However, to keep this work focused, we limited our study to the case of ^{18}F-FDG PET.

The following of this section discusses the results obtained in terms of quantification and registration outcomes.

A. *Quantification*

As shown in previous literature, the use of an attenuation map that is mismatched to the corresponding, un-gated PET dataset induces artefacts that compromise the quantitative accuracy of the images under examination [29]–[31]. In the same studies, methods to circumvent the problem were proposed, namely shifting the AC dataset to better align with the PET dataset (similarly to what we call sh(AVGC-insp)), or to acquire an AC CT that spans over multiple respiratory positions (cine-CT, average CT). Those studies often showed improved results, in terms of reduced artefacts in the final un-gated PET datasets, when the latter technique was implemented.

The results presented in our study seem to confirm the previous findings, and provide a further insight on the effect of AC when a *gated* PET dataset is used instead. More specifically, although the artefacts produced by the use of different attenuation maps are not always visually striking, we noticed that the AC CT used does have an effect on the reconstructed activity within the LV of the emission image. If an AC CT had to be chosen for quantification purposes, it would be advisable to go for the AVGC-exp, if a(n almost) perfectly matching AC CT cannot be obtained with the available instrumentation. In case of a mismatch in respiratory phase in the AC CT, a preliminary (manual or automatic) alignment of the myocardium is advisable before attenuation correction.

The artefacts highlighted in our study, when an average CT is used, are somehow more striking than what was previously documented in literature. This could be explained by the fact that our PET dataset is gated, hence represents one single cardiac and respiratory state of the patient. Correcting such dataset with an ACF sinogram derived from an AC CT that spans over multiple respiratory and/or cardiac cycles is by all means an approximation, which can introduce artefacts as likely as any other mismatched AC CT. In other words, such averaging introduces a mismatch between the temporal resolution of the PET (which, after gating, accounts only for one precise respiratory and cardiac phase) and the temporal resolution of the CT, now spanning over the full respiratory cycle. The studies mentioned above, on the other side, apply AC to non-gated PET datasets. It is therefore logical that such 'averaged' PET datasets, corrected with an ACF sinogram derived from an averaged AC CT, overall show a lower degree of artefacts.

B. *Registration*

The artefacts caused by breathing motion mislead the registration algorithm by producing a maximum mutual information for incorrectly aligned images. This result suggests that performing attenuation correction on the PET datasets can be deleterious for subsequent PET-to-HRCT registration if the respiratory phase of the attenuation map is not matching the respiratory phase of the PET gate. This happens regardless of the initial alignment between the emission and the anatomical dataset, thus suggesting that the AC strategy per se can hamper correct registration. In other words, even in the ideal case where no differences in patient positioning or body habitus can be found between the two datasets of interest, the PET-to-HRCT registration would fail if the AC CT was poorly chosen. Even if the patient positioning (and therefore the position of the internal organs relative to each other) were to differ slightly between scans, this is not expected to hamper the regis outcome since the cropping applied would mask out these differences. We assume that when the cardiac phase is matched, rigid registration suffices to align the cropped hearts.

Given that the choice of the correct respiratory phase seems to be important for proper attenuation correction and subsequent PET-to-HRCT registration, the following alternatives for AC are possible:

- an AC CT that almost perfectly matches the respiratory phase of the PET gate being reconstructed. Although this is the way to achieve the best and most stable registration results, this procedure would require the acquisition of a CT in a controlled respiratory phase (which would ask for some additional way to monitor or control the breathing [18]); if not, artefacts that might hamper subsequent registration will appear.
- an AC CT acquired over one or more cardiac phases and in any (fixed) respiratory phase, subsequently aligned to the PET dataset of interest (as in sh(AVGC-insp)).
- an AC CT acquired over one or more cardiac and respiratory phases, with low radiation burden for the

patient. In this case, the non-attenuation corrected PET dataset should be used for registration to the HRCT (after a preliminary rough alignment to it, if necessary). After PET-to-HRCT registration, a pasted-HRCT could be used for AC. This option could be particularly useful if the patient is not able to hold his breath in a fixed respiratory phase for a time sufficient to acquire the CT scan.

NOATTEN datasets: Without attenuation correction, significant artefacts can occur on the final PET reconstructions, including e.g. increased activity at the edges of the objects or increased activity in tissues of relatively low attenuation (eg. lungs). Therefore, the use of NOATTEN datasets for accurate registration was not an obvious choice. However, according to the results obtained from our XCAT simulations, confirmed by visually inspecting the results of the sheep datasets, a non-AC PET would serve the registration purpose much more efficiently than e.g. an attenuation map that spans over multiple breathing phases, provided that the datasets of interest are properly initialized. Once this is achieved, the registration of NOATTEN datasets yields registration results comparable to the ones obtained using a perfectly matching attenuation map, even in the presence of noise (cfr. C1-exp and NOATTEN in Fig. 8). This behavior differs from the case where other AC CTs (eg. AVGC-AVGR, C1-insp, ..) were used. In fact, even after a preliminary alignment of such AC PET datasets and the HRCT, the subsequent automatic registration to the HRCT drifted the PET away from its optimal position. The registration failed due to the artefacts present in such PET datasets, no matter how good the initial alignment is. The advantage of using NOATTEN datasets lies in the reduced burden for the patient, who would be relieved from holding his breath during the acquisition of the low dose AC CT. The attenuation correction of the PET dataset could be improved by pasting the registered HRCT, also used as anatomical prior, into such a full-FOV AC CT. This procedure would improve quantification, as the simulations in Section III-B report.

sh(AVGC-insp) datasets: The registrations obtained with the sh(AVGC-insp) technique, already implemented on many PET/CT systems, are confirmed to be almost as good as the ones obtained with a perfectly matching attenuation map, with the substantial advantage of being easier and more patient-friendly to acquire. In fact, most patients can be asked to hold their breath in a non-predefined respiratory phase for the time of the AC CT acquisition, and no control over the cardiac cycle is needed.

The sh(AVGC-insp) procedure only requires little user interaction, namely checking the alignment of a fast (dual-gated) PET reconstruction to the corresponding AC CT, which can possibly be substituted by an automatic registration procedure. Moreover, it has the advantage of being relatively robust to noise and to different initial positions of the HRCT (see Fig. 10).

Although this research covers various aspects of the problems introduced by AC in a doubly-gated PET scan on which PVC needs to be performed, the study has a few limitations that need to be discussed.

In the first place, we assume an ideal-case scenario where the patient has a shallow, regular breathing and beating pattern, in order to rule out any possible influence of the gating technique or of the pattern of the biological traces on the results obtained, and to demonstrate the effect of a motion-affected attenuation map, even when e.g. an ideal breathing or beating pattern are considered. Shallow breathing was here simulated since it is the most relevant for the clinic. It is known that, in real measurements, variable breathing patterns can be encountered [32]. The gating of the PET or the CT datasets of such patients would be influenced by such variability by increasing the inter-frame motion encountered. In addition, the patient might move during the PET scan, further degrading the final gated images. Although this effect is unavoidable, reducing the scan times could represent a solution to at least minimize the chances of occurrence of gross patient motion. Moreover, it is up to the gating technique of choice to be able to cope with such differences in the biological traces, and to possibly correct for other types of motion before reconstruction. The results here presented might worsen, in case the motion correction technique did not properly correct for all the motion within the PET frame of interest, but a study on the effect of gating on the subsequent registration to the HRCT is beyond the scope of this paper.

Also, the present study does not attempt to implement any motion compensation during reconstruction, to improve the statistics of the PET datasets. However, in the light of the simulations here performed at different noise levels, we believe that an image with better statistics would not dramatically improve the registration outcome. Moreover, in the case where attenuation is not jointly estimated during the PET reconstruction, we believe that the questions addressed by this study would remain even in the case of motion compensated PET images. In fact, if we assume that the respiratory motion compensation was performed using motion parameters obtained from the registration of different respiratory gates to a reference gate, we would need a sufficiently well-aligned attenuation map for every individual PET gate, in order to avoid the artefacts introduced by AC. If this was not the case, such artefacts might hamper the accurate registration of the different PET gates to the reference gate as much as they do when registering the PET to the HRCT, thus possibly impairing the respiratory motion estimation and subsequent compensation.

Regarding the adherence of the present work to a realistic scenario, a first comment goes for the simulated PET scanner. The Siemens Hirez PET scanner, despite its lack of time-of-flight (TOF) capabilities, is still in use for clinical routine work in many centres and has a spatial resolution comparable to most non-TOF PET/CT scanners. In TOF-PET, the problem of attenuation is less stringent thanks to the recent developments of MLAA and MLACF algorithms for joint estimation of activity and attenuation [33] [34]. In all non-TOF PET scanners however, which are still widespread and otherwise well-performing, the attenuation problem still remains.

Secondly, no noise was added to the simulated CT images, as its effect on the reconstruction and registration is considered negligible, if compared to the high noise level in the PET data.

A possible limitation of this study is that the cropping of

the images before registration is performed manually. Even if such manual step requires very little user interaction, a possible improvement would be to develop an algorithm for automatic cropping of the datasets to be registered.

Finally, in this study, a homogeneous distribution of the tracer in the LV was simulated (i.e. no areas of infarction). Even though studying an inhomogeneous distribution of the tracer might be more interesting from a medical point of view, a possible drawback of such simulated scenario would be a more difficult image registration, due to the infarction area, visible in the emission image but not on the HRCT. In this case, the registration might fail or perform worse not due to the sole effect of attenuation, but possibly also because of the characteristics of the datasets under examination. The use of an homogeneous distribution of activity, instead, allowed us to rule out any other cause of mis-registration except attenuation. In addition, it enabled the study of erroneous inhomogeneous uptake, which was solely caused by AC errors and different for the different AC maps used.

V. Conclusions

In this work, the effect of the use of different attenuation correction strategies on the subsequent registration between a dual-gated cardiac PET/CT and a HRCT acquired on a dedicated scanner was assessed. This registration procedure is a necessary step, if the aim is to reconstruct the PET dataset with high-resolution anatomical a-priori information.

The use of an attenuation map that perfectly matches the corresponding respiratory gate of the PET image is necessary to guarantee acceptable alignment between the PET gate and the HRCT. The blurring introduced by the beating heart, in contrast, does not influence the subsequent PET-to-HRCT registration and does not hamper left-ventricular quantification.

If the AC CT is not acquired in the same respiratory phase as the PET, it is necessary to first align it to the PET before proceeding to the attenuation correction step. This procedure clearly improves the registration results as well as the quantification of the uptake in the left ventricle. If only an AC CT is available that is corrupted by respiratory motion blur, the best alignment can be obtained by registering the non-attenuation-corrected PET to the HRCT. Once an aligned HRCT is obtained, usually only partially covering the full FOV, it can then be pasted into the blurred AC CT for attenuation correction to improve the left ventricular quantification and uniformity.

The results obtained with the simulations are confirmed in a proof-of-principle sheep experiment.

VI. Acknowledgements

Anna Turco is a PhD fellow of the Research Foundation - Flanders (FWO). Olivier Gheysens and Jens-Uwe Voigt are senior clinical investigators of the Research Foundation - Flanders. Kathleen Vunckx is a post-doctoral researcher of the Research Foundation - Flanders.

The authors wish to thank C. Watson, J. Jones et al. for their help with the Siemens data processing.

References

[1] M. J. Knuuti, P. Nuutila, U. Ruotsalainen, M. Ters, M. Saraste, R. Hrknen, A. Ahonen, U. Wegelius, A. Haapanen, and J. Bergman, "The value of quantitative analysis of glucose utilization in detection of myocardial viability by PET." *J Nucl Med*, vol. 34, no. 12, p. 206875, Dec. 1993.

[2] M. Dawood, F. Buther, N. Lang, O. Schober, and K. P. Schafers, "Respiratory gating in positron emission tomography: A quantitative comparison of different gating schemes," *Medical Physics*, vol. 34, no. 7, p. 3067, Jun. 2007.

[3] K. Thielemans, P. Schleyer, P. Marsden, R. Manjeshwar, S. Wollenweber, and A. Ganin, "Comparison of different methods for data-driven respiratory gating of PET data," in *Nuclear Science Symposium and Medical Imaging Conference (NSS/MIC), 2013 IEEE*, Oct 2013, pp. 1–4.

[4] F. Lamare, M. Ledesma Carbayo, T. Cresson, G. Kontaxakis, A. Santos, C. Le Rest, A. Reader, and D. Visvikis, "List-mode-based reconstruction for respiratory motion correction in PET using non-rigid body transformations." *Phys Med Biol.*, vol. 7, no. 52(17), pp. 5187–204, Sep.

[5] A. M. Alessio and P. E. Kinahan, "Improved quantitation for PET/CT image reconstruction with system modeling and anatomical priors." *Med Phys*, vol. 33, p. 4095:4103, 2006.

[6] K. Vunckx, A. Atre, K. Baete, A. Reilhac, C. M. Deroose, K. Van Laere, and J. Nuyts, "Evaluation of three MRI-based anatomical priors for quantitative PET brain imaging." *IEEE Trans Med Imaging*, vol. 31, no. 3, p. 599612, Mar. 2012.

[7] J. Cheng-Liao and J. Qi, "PET image reconstruction with anatomical edge guided level set prior," *Phys Med Biol*, vol. 56, no. 21, p. 6899, 2011.

[8] G. Mok, T. Sun, T.-C. Huang, and M. I. Vai, "Interpolated average CT for attenuation correction in PET-A simulation study," *IEEE Trans on Biomed Engineering*, vol. 60, no. 7, pp. 1927–1934.

[9] W. P. Segars, G. Sturgeon, S. Mendonca, J. Grimes, and B. Tsui, "4D XCAT phantom for multimodality imaging research." *Med Phys*, vol. 37, no. 9, p. 4902:15, 2010.

[10] R. Boellaard, "Standards for PET Image Acquisition and Quantitative Data Analysis." *J Nucl Med*, vol. 50, no. Suppl 1, p. 11:20, 2009.

[11] W. van Elmpt, J. Hamill, J. Jones, D. De Ruysscher, P. Lambin, and M. llers, "Optimal gating compared to 3D and 4D PET reconstruction for characterization of lung tumours," *European Journal of Nuclear Medicine and Molecular Imaging*, vol. 38, no. 5, pp. 843–855, 2011.

[12] A. Martinez-Möller, M. Souvatzoglou, N. Navab, M. Schwaiger, and S. Nekolla, "Artifacts from misaligned CT in cardiac perfusion PET/CT studies: frequency, effects, and potential solutions." *J Nucl Med*, vol. 48, no. 2, pp. 188–93, Feb 2007.

[13] K. Khurshid, R. J. McGough, and K. Berger, "Automated cardiac motion compensation in pet/ct for accurate reconstruction of pet myocardial perfusion images," *Physics in Medicine and Biology*, vol. 53, no. 20, p. 5705, 2008.

[14] M. Brambilla, C. Secco, M. Dominietto, R. Matheoud, G. Sacchetti, and E. Inglese, "Performance Characteristics Obtained for a New 3-Dimensional Lutetium OxyorthosilicateBased Whole-Body PET/CT Scanner with the NEMA NU 2-2001 Standard." *J Nucl Med*, vol. 46, no. 12, 2005.

[15] A. Turco, J. Nuyts, O. Gheysens, J. Voigt, P. Claus, and K. Vunckx, "Registration between respiratory-gated pet/ct and high-resolution ct with xcat simulations: Evaluation and optimization for subsequent pvc," in *Nuclear Science Symposium and Medical Imaging Conference (NSS/MIC), 2013 IEEE*, Oct 2013, pp. 1–6.

[16] M. D. Cerqueira, N. Weissman, V. Dilsizian, A. Jacobs, S. Kaul, W. Laskey, D. Pennell, J. Rumberger, T. Ryan, and M. Verani, "Standardized myocardial segmentation and nomenclature for tomographic imaging of the heart a statement for healthcare professionals from the cardiac imaging committee of the Council on Clinical Cardiology of

the American Heart Association." *Circulation*, vol. 105.4, pp. 539–542, 2002.

[17] C. Studholme, D. L. G. Hill, and D. J. Hawkes, "An overlap invariant entropy measure of 3D medical image alignment." *Pattern Recognition*, vol. 32, p. 71:86, 1999.

[18] T. Sun, T.-H. Wu, S.-J. Wang, B.-H. Yang, N.-Y. Wu, and G. S. P. Mok, "Low dose interpolated average ct for thoracic pet/ct attenuation correction using an active breathing controller," *Medical Physics*, vol. 40, no. 10, pp. –, 2013.

[19] P. Kinahan, D. Townsend, T. Beyer, and D. Sashin, "Attenuation correction for a combined 3d pet/ct scanner," *Medical physics*, vol. 25, no. 10, pp. 2046–2053, 1998.

[20] F. Maes, A. Collignon, D. Vandermeulen, G. Marchal, and P. Suetens, "Multimodality image registration by maximization of mutual information," *IEEE Trans Med Imaging*, vol. 16, no. 2, pp. 187–198, Apr 1997.

[21] R. Shekhar, V. Walimbe, S. Raja, V. Zagrodsky, M. Kanvinde, G. Wu, and B. Bybel, "Automated 3-dimensional elastic registration of whole-body pet and ct from separate or combined scanners," *Journal of Nuclear Medicine*, vol. 46, no. 9, pp. 1488–1496, 2005.

[22] M. R. Patel, R. D. White, S. Abbara, D. A. Bluemke, R. J. Herfkens, M. Picard, L. J. Shaw, M. Silver, A. E. Stillman, and J. Udelson, "2013 ACCF/ACR/ASE/ASNC/SCCT/SCMR Appropriate utilization of cardiovascular imaging in heart failure. A joint report of the American College of Radiology, Appropriateness Criteria Committee and the American College of Cardiology Foundation Appropriate Use Criteria Task Force," *Journal of the American College of Cardiology*, vol. 61, no. 21, pp. 2207–2231, 2013.

[23] L. J. Anderson, C. Miyazaki, G. R. Sutherland, and J. K. Oh, "Patient selection and echocardiographic assessment of dyssynchrony in cardiac resynchronization therapy," *Circulation*, vol. 117, no. 15, pp. 2009–2023, Apr 2008.

[24] J. A. Jarcho, "Biventricular pacing," *New England Journal of Medicine*, vol. 355, no. 3, pp. 288–294, 2006.

[25] B. Nowak, A. M. Sinha, W. M. Schaefer, K. C. Koch, H. J. Kaiser, P. Hanrath, U. Buell, and C. Stellbrink, "Cardiac resynchronization therapy homogenizes myocardial glucose metabolism and perfusion in dilated cardiomyopathy and left bundle branch block," *J. Am. Coll. Cardiol.*, vol. 41, no. 9, pp. 1523–1528, May 2003.

[26] K. Russell, M. Eriksen, L. Aaberge, N. Wilhelmsen, H. Skulstad, E. W. Remme, K. H. Haugaa, A. Opdahl, J. G. Fjeld, O. Gjesdal, T. Edvardsen, and O. A. Smiseth, "A novel clinical method for quantification of regional left ventricular pressure–strain loop area: a non-invasive index of myocardial work," *European Heart Journal*, 2012.

[27] D. Birnie, R. A. deKemp, T. D. Ruddy, A. S. Tang, A. Guo, K. Williams, R. Wassenar, M. Lalonde, and R. S. Beanlands, "Effect of lateral wall scar on reverse remodeling with cardiac resynchronization therapy," *Heart Rhythm*, vol. 6, no. 12, pp. 1721 – 1726, 2009.

[28] "Flash speed. Lowest dose. SOMATOM Definition Flash." http://www.radiology.vcu.edu/docs/CT_Definition_Flash.pdf, 2009, [Online].

[29] A. M. Alessio, S. Kohlmyer, K. Branch, G. Chen, J. Caldwell, and P. Kinahan, "Cine CT for attenuation correction in cardiac PET/CT," *J. Nucl. Med.*, vol. 48, no. 5, pp. 794–801, May 2007.

[30] T. Pan, O. Mawlawi, S. A. Nehmeh, Y. E. Erdi, D. Luo, H. H. Liu, R. Castillo, R. Mohan, Z. Liao, and H. A. Macapinlac, "Attenuation correction of PET images with respiration-averaged CT images in PET/CT," *J. Nucl. Med.*, vol. 46, no. 9, pp. 1481–1487, Sep 2005.

[31] K. L. Gould, T. Pan, C. Loghin, N. P. Johnson, A. Guha, and S. Sdringola, "Frequent diagnostic errors in cardiac PET/CT due to misregistration of CT attenuation and emission PET images: a definitive analysis of causes, consequences, and corrections," *J. Nucl. Med.*, vol. 48, no. 7, pp. 1112–1121, Jul 2007.

[32] C. Liu, L. Pierce, A. Alessio, and P. Kinahan, "The impact of respiratory motion on tumor quantification and delineation in static PET/CT imaging." *Phys Med Biol*, vol. 54, no. 24, pp. 7345–62.

[33] A. Rezaei, M. Defrise, and J. Nuyts, "ML-reconstruction for TOF-PET with simultaneous estimation of the attenuation factors," *IEEE Trans Med Imaging*, vol. 33, no. 7, pp. 1563–1572, Jul 2014.

[34] A. Rezaei, M. Defrise, G. Bal, C. Michel, M. Conti, C. Watson, and J. Nuyts, "Simultaneous reconstruction of activity and attenuation in time-of-flight PET," *IEEE Trans Med Imaging*, vol. 31, no. 12, pp. 2224–2233, Dec 2012.